Analysis of Mechanical Properties of Iron Roughneck's Spin-Rollers

Yongbai Sha[1(✉)], Quan Li[1], and Xiaoying Zhao[2]

[1] School of Mechanical and Aerospace Engineering, Jilin University, Changchun, China
shayb@jlu.edu.cn
[2] Changchun Vocational Institute of Technology, Changchun, China

Abstract. The spinner mechanism of the iron roughneck is used to realize the rapid screwing in or screwing out of the drill pipe thread. The spin-rollers are one of the main components of the spinner mechanism, which directly contacts the drill pipe and applies clamping force and torque to the drill pipe. Good mechanical performance is the premise to ensure its reliable work. In this paper, the structure and working principle of the spinner mechanism are introduced. The spinner mechanism adopts a new type of spin-rollers, which makes the structure of the mechanism more compact and better restricts the position of the drilling tool. In order to ensure the mechanical performance of the spinning roller, the stress analysis of the spinner mechanism and the drill pipe is conducted, and the force between the roller and the drill pipe and the required oil cylinder thrust are obtained. According to the obtained force, the finite element simulation analysis of the spin-rollers and drill pipe is carried out, and the distribution of stress and deformation is obtained. The analysis results show that the designed spin-rollers meets the requirements of mechanical properties.

Keywords: Iron roughneck · Spin-roller · mechanical properties · finite element analysis

1 Introduction

With the demand of modern drilling operation, the requirements for the automation of drilling operation are gradually increased [1, 2]. Iron roughneck is the wellhead operation equipment to realize the automatic makeup and shackle operation of drilling tools, and its application is more and more common [3, 4]. The spinner mechanism is one of the main working mechanisms of the iron roughneck, which is used to realize the rapid screwing in and screwing out of the drilling tool thread, and the spin-rollers are the direct force bearing part of the spinner mechanism [5]. Good mechanical performance is the premise to ensure its reliable work. The mechanical performance of the spin-rollers is analysed in this paper.

L. Yan and J. Na (Eds.): ICFPMCE 2022, AHE 10, pp. 393–404, 2023.
https://doi.org/10.2991/978-94-6463-022-0_33

2 Working Principle of the Spinner Mechanism

The three-dimensional model of the spinner mechanism is shown in Fig. 1, which is mainly composed of clamping oil cylinder, cross beam, wedge plate, return spring, tangent wheel, follow-up roller, clamping arm, driving roller, hydraulic motor, and upright column. The cylinder body of the clamping oil cylinder is hinged with the cross beam, and the piston rod is connected with the wedge plate. The tangent roller is installed on the pin shaft at the end of the clamping arm and can roll along the edge of the wedge plate. The return spring is used to limit the position of the clamping arm, keep the tangent roller at the end of the clamping arm in contact with the edge of the wedge plate, and the clamping arm can open automatically when the piston rod of the clamping oil cylinder retracts. The spin-rollers include two driving rollers and two groups of follow-up rollers installed on the roller frame. The driving roller is driven to rotate by the hydraulic motor, and the follow-up roller is used for limit and auxiliary support. This type of spin-rollers can not only meet the requirements of spin torque, but also better restrict the position of the drilling tools to achieve smooth spinning. A floating mechanism is installed between the cross beam and the upright column. When subjected to external force, the cross beam can float back or forth along the guide rail on the upright column to adapt to the position of the drill pipe.

When working, the piston rod of the clamping oil cylinder extends to push the wedge plate to drive the follow-up rollers to approach the drill pipe. At the same time, the two sides of the wedge plate push the tangent wheel installed at one end of the clamping arm to swing outward, and then driving the clamping arm to rotate around the middle pin shaft, to realize the inward rotation of the driving roller installed at the other end of the clamping arm. This form of spinner mechanism reduces the number of clamping oil cylinders and has a compact structure. However, when working, the driving rollers

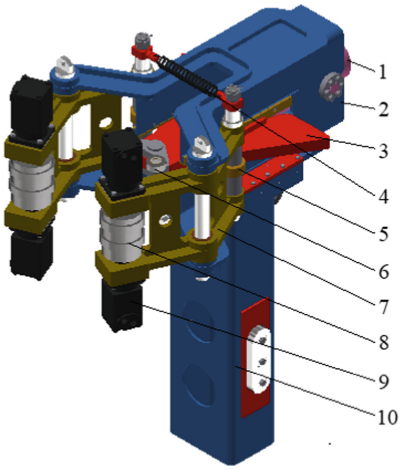

Fig. 1. Spinner mechanism. In the figure: 1-clamping oil cylinder, 2-cross beam, 3-wedge plate, 4-return spring, 5-tangent wheel, 6-follow-up roller, 7-clamping arm, 8-driving roller, 9-hydraulic motor, 10-upright column.

and the following rollers will not contact the drilling tool at the same time. When the roller in one direction contacts the drilling tool, the contact force will be generated. Due to the action of the floating mechanism, the whole spinner mechanism outside the upright column will move back or forth under the action of force until all the spin-rollers completely clamp the drilling tool. When the spin-rollers clamp the drilling tool, the hydraulic motor drives the driving roller to rotate, to drive the drilling tool to rotate clockwise or anti-clockwise to complete the rapid screwing in or screwing out of the drilling tool thread.

3 Calculation of Clamping Force and Oil Cylinder Thrust

The maximum spin torque of the spinner mechanism is $M_{\max} = 2373$ Nm, which corresponds to the drill tool with a diameter of 311 mm. During spinning, the resistance between the follow-up rollers and the drilling tool and the force generated by the return spring are small and ignored. When the holding force of the spinner mechanism is the maximum, the tangent rollers are at the limit position on both sides of the wedge plate near the follow-up rollers. The stress diagram of the mechanism when clamping the drill tool with a diameter of 311 mm is shown in Fig. 2. The spinner mechanism is symmetrical. In order to make the analysis diagram concise and clear, only the force on one side is drawn in the diagram, and the other side is symmetrical and not drawn.

Taking the components composed of clamping arm, driving roller and tangent wheel as the research object, the torque equation of point K is as follows:

$$F_a d_a = F_b' d_b \tag{1}$$

Where, F_a is the force exerted by the wedge plate on the tangent wheel; F_b' is the force exerted by the drill pipe on the driving roller, which is the reaction force of F_b,

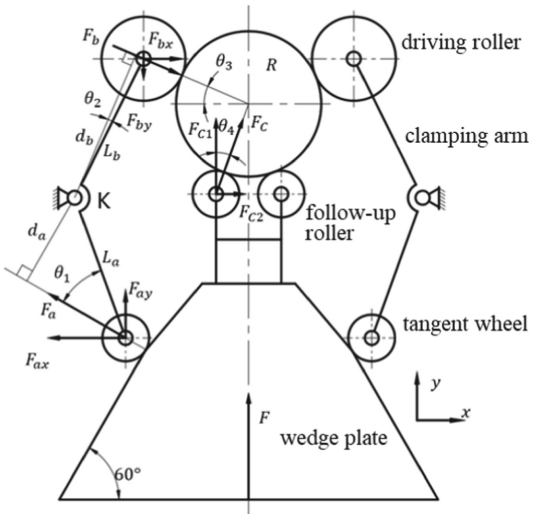

Fig. 2. Calculation diagram of clamping force

and F_b is the force exerted by the driving roller on the drill pipe; d_a and d_b are the force arms of the force F_a and F_b' relative to the hinge point K of the clamping arm. The relationship between d_a, d_b and the lengths L_a, L_b of the clamping arm is as follows:

$$\begin{cases} d_a = L_a \sin\theta_1 \\ d_b = L_b \cos\theta_2 \end{cases} \tag{2}$$

The spin torque M_{max} applied by the driving roller on the drilling tool is as follow:

$$M_{max} = 2\mu F_b R \tag{3}$$

Where, μ is the friction coefficient and R is the drilling tool radius. According to the materials of the drilling tools and the rollers, the friction coefficient between them is about 0.2 [6].

The force balance equation of the drill tool in y direction is as follow:

$$F_{by} + F_{C1} = 0 \tag{4}$$

Where:

$$F_{by} = F_b \sin\theta_3, F_{C1} = F_C \cos\theta_4 \tag{5}$$

Where, F_{by} and F_{C1} are the components of F_b and F_C in the y direction respectively, and F_C is the force of the follow-up roller on the drill pipe.

The stress equation in the y direction of the wedge plate is as follow:

$$F - 2F'_{C1} - 2F'_{ay} = 0 \tag{6}$$

Where, F is the thrust of the oil cylinder, F_{C1}' is the reaction force of F_{C1}, F_{ay}' is the component force in y direction which exerted by the one-sided tangent wheel on the wedge plate, and F_{ay}' is the reaction force of F_{ay}, and its size is:

$$F'_{ay} = F_{ay} = F_a \cos 60° \tag{7}$$

The values of relevant parameters are shown in Table 1.

Table 1. Parameter values

Parameter	Value
L_a	320 mm
L_b	332 mm
θ_1	40.77°
θ_2	0.91°
θ_3	26.15°
θ_4	21.56°
R	155.5 mm

Simultaneous formula (1)–formula (7) and substituting the data in Table 1, the following results can be obtained: $F_a = 60605$ N, $F_b = 38151$ N, $F_c = 18079$ N; $F_{c1} = 16814$ N, $F_{ay} = 30302.5$ N, $F_{by} = 16814$ N; and the required hydraulic cylinder thrust is $F = 94233$ N.

4 Simulation Analysis

In the process of spinning, the spin-rollers clamp the drilling tool and generate friction, and the torque is transmitted through the contact friction [7, 8]. In this paper, ABAQUS software is used for simulation analysis. By establishing the finite element simulation model of the spin-rollers and the drilling tool, and analysing and calculating, the stress and deformation caused by the contact between the spin-rollers and the drilling tool can be obtained, and the mechanical properties of the spin-rollers can be verified.

4.1 Establishment of Simulation Model

This paper focuses on the force generated by the interaction between the spin-rollers and the drilling tool. In order to improve the calculation speed, the three-dimensional model used in the simulation does not need to import the complete iron roughneck's spinner mechanism, but only the three-dimensional model of the contact section of the drilling tool, the driving rollers, and the follower-up rollers. The imported three-dimensional model is shown in Fig. 3. In the Fig. 3, the diameter of the drilling tool is 311 mm. In this case, the force required to hold the drilling tool is the largest, so the stress generated by the contact of each component is also the largest.

4.2 Mesh Division and Material Attribute Assignment

Considering the accuracy of analysis and calculation and the rapidity of calculation, the mesh division is distinguished according to the stress of each component and the different contact area during spinning. The contacts between the drilling tool and the driving rollers and the follow-up rollers are only in a small range, so the mesh in the contact area between the drilling tool and the rollers is densified, and the mesh in other

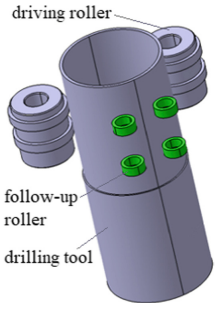

Fig. 3. Simulation model

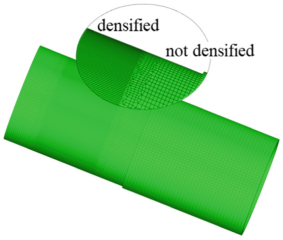

Fig. 4. Mesh division of drilling tool

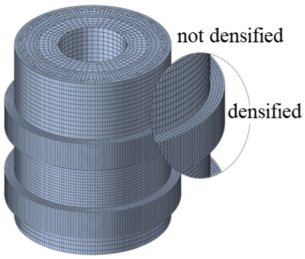

Fig. 5. Mesh division of driving roller

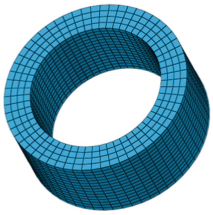

Fig. 6. Mesh division of follow-up roller

positions is sparse. The focus area of the driving roller is the contact force between the lugs of the roller and the drilling tools. Therefore, the mesh is densified for the lugs while the mesh for the rest is not densified. The simplified structure of the follow-up roller is a circle and the mesh does not need to be differentiated. Figures 4, 5 and 6 show the meshing of the drilling tool, the driving roller, and the follow-up roller respectively. The number of mesh units of the drilling tool is 248112, and the unit type is a mixture of tetragonal pyramid and hexahedron. The mesh unit number of the driving roller is 104592, and the unit type is a mixture of tetragonal pyramid and hexahedron. The number of mesh units of the follow-up roller is 3600 and the unit type is hexahedron.

The assembly effect of the drilling tool, the driving rollers and the follower-up rollers after meshing is shown in Fig. 7. In the model, the material density of each component is 7.9×10^3 kg/m^3, the elastic modulus is 210 GPa and the Poisson ratio is 0.3. The section properties of each component are set as uniform distribution of a single material.

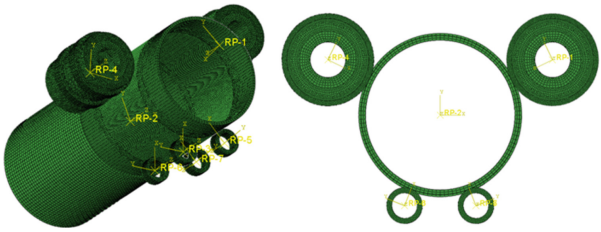

Fig. 7. Model import and assembly

4.3 Adding Constraints and Loads

4.3.1 Constraint Settings

The simulation is divided into initial step and loading step 1. The initial step is the contact-generated analysis step, so all components are constrained to the full degree of freedom in this step. Constraints are added to each component by referring to the assembly relationship in the three-dimensional model of the iron roughneck and the process of tightening. The driving roller releases x-axis of its reference coordinate system in step 1, which is the degree of freedom of translation relative to the radial direction of the drill tool. In step 1, the drilling tool releases the degree of freedom of translation along the x-axis and y-axis of its coordinate system. The follow-up roller limits its full degree of freedom in step 1.

4.3.2 Load Settings

According to the calculation above, the force between the driving roller and the drilling tool is $F_b = 38151$ N, pointing to the drilling tool axis along the axis of the driving roller, which is the x-axis direction of the reference coordinate system of the driving roller. This force is set as the driving roller load and added to the coupling reference point established.

4.3.3 Contact Settings

For each component in the simulation, the attributes are Surface to Surface type when contacting, the friction coefficient is 0.2, and the other attributes are default settings. There are six contact surfaces in the model, including two pairs of driving rollers - drilling tools and four pairs of follow-up rollers - drilling tools. In order to improve the astringency of calculation, the clearance tolerance of contact surface is set at 0.1mm.

4.4 Simulation Results and Analysis

After solving the simulation model, the assembly stress distribution diagram (Fig. 8a) and deformation distribution diagram (Fig. 8b) as shown in Fig. 8 are obtained. It can be seen that large stress and deformation basically appear in the contact area. The maximum stress in the assembly is 366 MPa and the maximum deformation is 0.3616 mm, which are located at the contact position between the spin-rollers and the drilling tool.

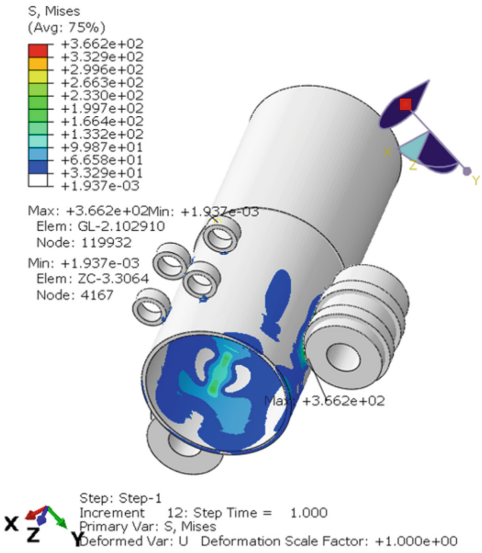

(a)

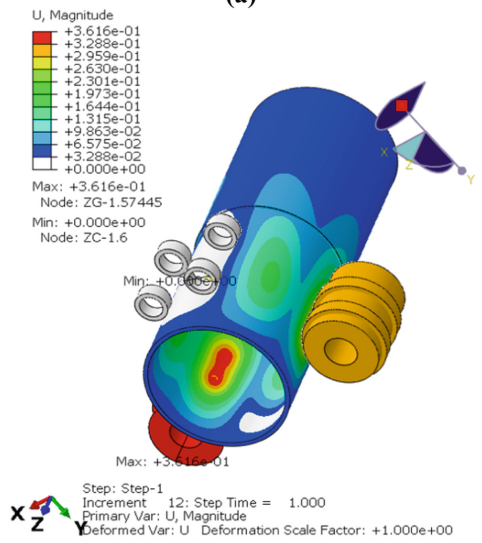

(b)

Fig. 8. Stress and deformation of the assembly: (a) Stress distribution diagram; (b) Deformation distribution diagram.

The stress distribution at the contact area of the drilling tool is shown in Fig. 9. The left figure shows the perspective of the drilling tool in contact with the follower-up rollers, and the right figure shows the perspective of the drilling tool in contact with the driving roller. It can be seen that the relatively large stress is distributed in the area in contact with two driving rollers and the area in contact with four follow-up rollers. The maximum value appears at the position in contact with the driving rollers, which is

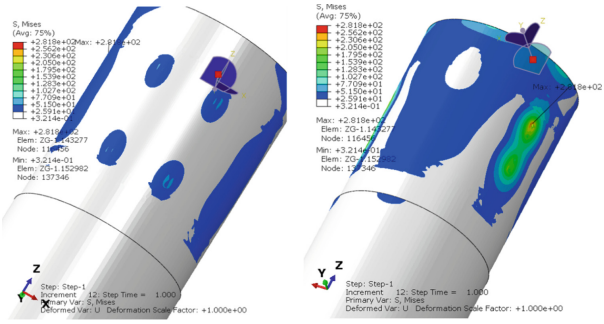

Fig. 9. Drilling tool stress distribution

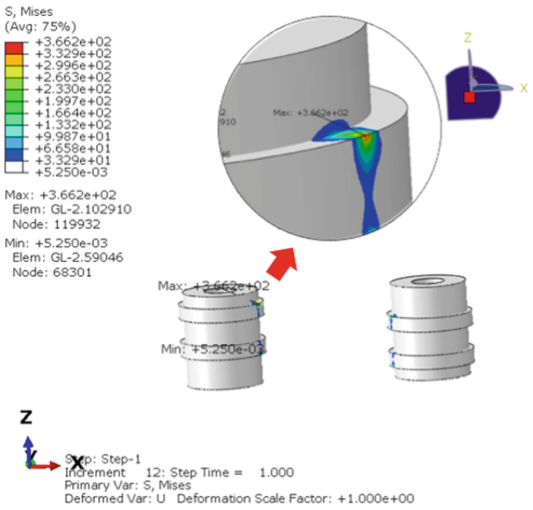

Fig. 10. Stress distribution of driving roller

281 MPa. It is less than the allowable stress of the drill pipe material 621 MPa, so the strength of the drill pipe meets the requirements.

The stress distribution of the driving rollers is shown in Fig. 10. The maximum stress appears at the edge of the boss, which is 366 MPa, and less than the allowable stress of the material 523 MPa. Therefore, the strength of the driving roller meets the requirements.

The stress distribution of the four follow-up rollers is shown in Fig. 11. Their stress distribution forms are basically the same. The maximum stress value appears at the edge of the rollers, which is 92.85 MPa, less than the allowable stress of the material 523 MPa. Therefore, the strength of the driving roller meets the requirements.

In conclusion, the designed driving rollers and follow-up rollers meet the strength requirements, and the force exerted by the rollers will not damage the drill pipe. According to the situation that the maximum stress appears at the edge of the boss of the driving rollers and the edge of the follow-up rollers, it can be seen that there is stress concentration at this part. The stress condition can be further improved and the overall service

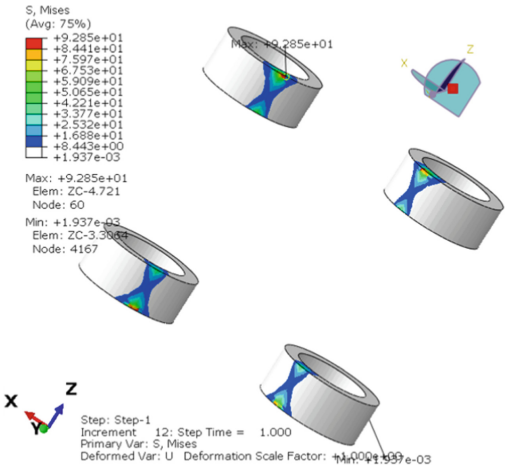

Fig. 11. Stress distribution of follow-up roller

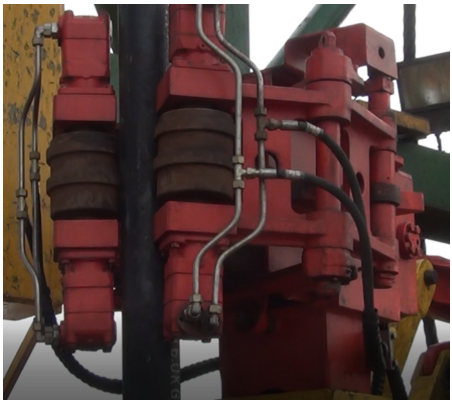

Fig. 12. Working photo of spinner mechanism

performance can be improved by machining the transition fillet at the corresponding position. Figure 12 is the working photo of the spinner mechanism. The application shows that the spin-rollers can reliably clamp the drill pipe, and the spin torque meets the design requirements, and the rollers and drill pipe are not damaged.

5 Conclusions

A new type of iron roughneck's spinner mechanism is designed in this paper. The spin-rollers of the mechanism consist of two driving rollers and two groups of follow-up rollers installed on the roller frame. The clamping action of the driving rollers uses wedge plate force transmission mechanism. This form of spinner mechanism reduces the number of clamping cylinders and makes the overall structure of the spinner mechanism more

compact while meeting the requirements of spin torque and restricting drilling tool position. The spinner mechanism uses the hydraulic motor to drive the driving rollers to rotate, and drives the drill pipe to rotate through the friction between the driving rollers and the drill pipe, to realize the screwing in and screwing out of the drill pipe thread. The sufficient clamping force of the rollers on the drill pipe is the prerequisite to realize this function. According to the requirements of the spin torque, the mechanical analysis is carried out, and the force of the driving rollers and follow-up rollers on the drilling tool and the required thrust of clamping oil cylinder are obtained. According to the calculation results, the simulation analysis is carried out by using the finite element simulation software, and the stress distribution and deformation distribution of the driving rollers, the follower-up rollers and the drilling tool are obtained. The simulation results show that the designed spin-rollers mechanism meets the application requirements.

Acknowledgments. This research was funded by the Ministry of Land and Resources of China, grant number SinoProbe-09-05; China Geological Survey, grant number 12120113017600; and Program for JLU Science and Technology Innovative Research Team, grant number 2017TD-13.

Authors' Contributions. Conceptualization, Y.S. and Q.L.; methodology, Y.S. and Q.L.; software, Y.S.and Q.L.; validation, Y.S., Q.L. and X.Z.; formal analysis, Y.S. and X.Z.; investigation, Y.S. and Q.L.; resources, Y.S., Q.L. and X.Z.; data curation, Y.S. and Q.L.; writing—original draft preparation, Y.S.; writing—review and editing, Y.S., Q.L. and X.Z.; visualization, Q.L.; supervision, Y.S.; project administration, Y.S.; funding acquisition, Y.S. All authors have read and agreed to the published version of the manuscript.

References

1. Ramba, V., Selvaraju, S., Subbiah, S., Palanisamy, M., Srivastava, A.: Optimization of drilling parameters using improved play-back methodology. J. Pet. Sci. Eng. **206**, 108991 (2021). https://doi.org/10.1016/j.petrol.2021.108991
2. Godhavn, J.M., Pavlov, A., Kaasa, G.O., Rolland, N.L.: Drilling seeking automatic control solutions. In: Proceedings of the 18th IFAC World Congress (IFAC 2011), Milano, Italy, 28 August–2 September 2011. https://doi.org/10.3182/20110828-6-IT-1002.00551
3. Sun, Y.H., Zhang, F.Y., Wang, Q.Y., Gao, K.: Application of "Crust 1" 10k ultra-deep scientific drilling rig in Songliao Basin Drilling Project (CCSD-SKII). J. Pet. Sci. Eng. **145**, 222–229 (2016). https://doi.org/10.1016/j.petrol.2016.04.003
4. Zhdaneev, O.V., Frolov, K.N., Petrakov, Y.A.: Predictive systems for the well drilling operations. In: Kravets, A.G., Bolshakov, A.A., Shcherbakov, M. (eds.) Cyber-Physical Systems: Design and Application for Industry 4.0. SSDC, vol. 342, pp. 347–368. Springer, Cham (2021). https://doi.org/10.1007/978-3-030-66081-9_28
5. Qin, D.T., Xie, L.Y.: Modern Mechanical Design Handbook, (vol. 1). Chemical Industry Press (2011)
6. Liu, J., Wen, Y.Q.: Analysis of the control strategy of the intelligent iron Roughneck's make-up and break-out fusion with fuzzy adaptive control algorithm. J. Phys. Conf. Ser. **1992**, 032099 (2021). https://doi.org/10.1088/1742-6596/1992/3/032099

7. Shah, D.B., Patel, K.M., Trivedi, R.D.: Analyzing Hertzian contact stress developed in a double row spherical roller bearing and its effect on fatigue life. Ind. Lubr. Tribol. **68**, 361–368 (2016). https://doi.org/10.1108/ILT-06-2015-0082
8. Hu, Z.J., Ma, Q.F., Liu, J.L.: Load analysis and calculation of makeup and breakout device on continuous circulation system. China Pet. Mach. **47**, 31–37 (2019). https://doi.org/10.16082/j.cnki.issn.1001-4578.2019.12.005